Journal of Biomechanics 50 (2017) 114–120

Contents lists available at ScienceDirect

Journal of Biomechanics

journal homepage: www.elsevier.com/locate/jbiomech
www.JBiomech.com

Development of a platelet adhesion transport equation for a computational thrombosis model

Joshua O. Taylor [a,b], Ling Yang [a], Steven Deutsch [b], Keefe B. Manning [a,c,*]

[a] Department of Biomedical Engineering, The Pennsylvania State University, University Park, PA, USA
[b] Applied Research Laboratory, The Pennsylvania State University, State College, PA, USA
[c] Department of Surgery, Penn State Hershey Medical Center, Hershey, PA, USA

ARTICLE INFO

Article history:
Accepted 2 November 2016

Keywords:
Thrombosis
Platelets
Modeling
Laser Doppler velocimetry
Adhesion
Computations

ABSTRACT

Thrombosis is a significant issue for cardiovascular device development and use. While thrombosis models are available, very few are device-related and none have been thoroughly validated experimentally. Here, we introduce a surface adherent platelet transport equation into a continuum model to account for the biomaterial interface/blood interaction. Using a rotating disc system and polyurethane-urea material, we characterize steady and pulsatile flow fields using laser Doppler velocimetry. In vitro measurements of platelet adhesion are used in combination with the LDV data to provide further experimental validation. The rotating disc system is computationally studied using the device-induced thrombosis model with the surface platelet adherent transport equation. The results indicate that the flow field is in excellent agreement to the experimental LDV data and that the platelet adhesion simulations are in good agreement with the in vitro platelet data. These results provide good evidence that this transport equation can be used to express the relationship between blood and a biomaterial if the correct platelet adhesion characteristics are known for the biomaterial. Further validation is necessary with other materials.

1. Introduction

Thrombosis often limits the widespread use of mechanical circulatory support devices, prosthetic valves, and other blood contacting devices (Daemen et al., 2007; Mehra et al., 2014; deBiasi et al., 2015; Marchena et al., 2015). Their design typically warrants extensive in vitro, hemocompatibility, animal, and clinical testing. While computational fluid dynamics (CFD) would ideally reduce the need for testing (Stewart et al., 2013) and the mathematical underpinnings of thrombosis models are available (Leiderman and Fogelson, 2014), there needs to be experimental validation of the models.

Groups have been developing computational thrombosis models focused on cellular interactions (Xu et al., 2011; Wang and King, 2012; Cito, 2013; Leiderman and Fogelson, 2014). While they have been able to grow a thrombus as a result of injury, most lack significant experimental validation. We recently published a device-induced thrombosis model using activated and non-activated platelets and ADP to grow a thrombus (Taylor et al., 2016). Experimentally acquired data of thrombi formed in an expansion using magnetic resonance imaging was used to test the model (Taylor et al., 2014). However, platelet adhesion was not included and is the focus here.

Platelet adhesion is a necessary precursor to macroscopic thrombus deposition and growth. Consequently, it is frequently used as a metric to assess device efficacy. There have been numerous modeling approaches for platelet adhesion, including Lagrangian approaches to more accurately simulate biomechanics on a cellular level (e.g., Mori et al., 2008; Fogelson and Guy 2008; Tokarev et al., 2011) or Eulerian approaches to better simulate larger spatial scales (e.g., Strong, 1987; Sorensen, 1999a; Goodman et al., 2005). Yet, no one has incorporated platelet adhesion into a thrombosis model capable of making quantitative predictions in three dimensions and on the spatial and temporal scales relevant to medical devices.

In an effort to integrate platelet adhesion into the thrombosis model from Taylor et al. (2016), we use in vitro platelet adhesion experiments from Navitsky et al. (2014) to calibrate a transport equation for surface adherent platelets (SAPs) under steady and pulsatile conditions. The in vitro platelet adhesion data were collected using polyurethane-urea (PUU): a clinically relevant biomaterial (Yamanaka et al., 2005). The blood-contacting properties

* Correspondence to: Department of Biomedical Engineering, The Pennsylvania State University, 205 Hallowell Building, University Park, PA 16802, USA. Fax: +1 814 863 0490.
E-mail address: kbm10@psu.edu (K.B. Manning).

http://dx.doi.org/10.1016/j.jbiomech.2016.11.012
0021-9290/

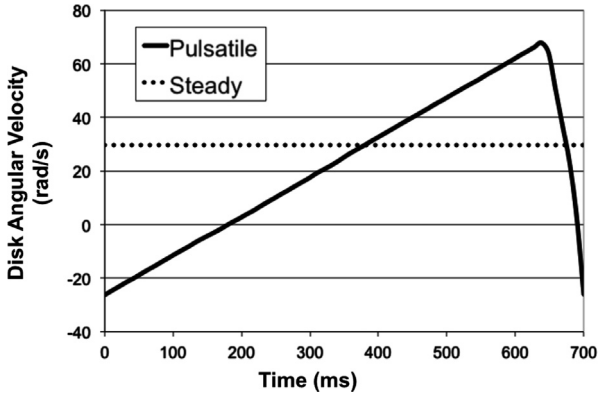

Fig. 1. The two waveforms used to control disc rotation. The pulsatile waveform has an RMS angular velocity of 29.63 rad/s (equal to the steady waveform) and has a clinically relevant period of 700 ms.

of PUU have been studied extensively (Milner et al., 2006; Topper et al., 2014).

The transport equation for platelet adhesion is based on Strong et al. (1987) and is added to the framework of a blood coagulation model developed by Fogelson (1992). A macroscopic and continuum framework is vital for making predictions of platelet adhesion on the spatial and temporal scales relevant to medical devices, as it eliminates the need to model prohibitively complex cellular interactions. Additionally, it allows the entire computational domain, even a growing thrombus, to be treated as a fluid, as demonstrated by Taylor et al. (2016).

In the present work, a rotating disc system (RDS), comparable to the experimental setup of Navitsky et al. (2014), is simulated and provides a means to assess model predictions of platelet adhesion. In an effort to isolate platelet adhesion, we focus on laminar conditions to eliminate the increase in complexity that would come along with turbulent flow. Nevertheless, our considered conditions encompass a wide range of physiologically relevant wall shear stresses (WSS), and we introduce a novel method for developing an SAP transport equation.

2. Methods

2.1. Experimental measurements

Platelet adhesion to PUU was studied using a rotating disk and is thoroughly described in Navitsky et al. (2014). In brief, a 20 mm diameter circle of smooth PUU was adhered to the bottom of a 20 mm diameter metallic disc. The disc was attached to a shaft and motor, suspended in a cylindrical, acrylic reservoir, and rotated according to four pulsatile and one steady waveforms, which yielded a wide range of physiologically relevant WSS on the disc surface. The reservoir was filled with bovine platelet rich plasma (PRP), reconstituted after centrifugation to maintain a constant platelet concentration of 350×10^6 platelets/mL, and the disc was rotated for two hours. Six experiments were performed for each waveform, and platelet adhesion data were collected at nine radial locations: 0, 1, 2, 3, 4, 5, 6, 7, 8, and 9 mm. SAP concentrations were quantified with confocal microscopy after fixation and fluorescent labeling of platelets. SAP concentration was calculated by counting adherent platelets within a 0.011 mm^2 interrogation region.

We discuss one steady and one pulsatile disc rotation (Fig. 1), which correspond to the steady and +25% ramp waveforms used in Navitsky et al. (2014). The steady waveform produces a constant rotation rate of 29.63 rad/s (283 RPM) and the pulsatile waveform maintains an RMS rotation rate of 29.63 rad/s. The pulsatile waveform produces minimum and maximum rotation rates of −26.3 and 68 rad/s, and angular accelerations of 150 and −1500 rad/s^2 on the up and down slopes. The pulsatile waveform has a period of 700 ms. The steady waveform Reynolds number (Re) is 1950, while the pulsatile waveform has a maximum Re and an RMS Re of 4500 and 1950, respectively.

To define the pulsatile flow field, laser Doppler velocimetry (LDV) data were collected every 1 mm along a radial line 100 μm beneath the disc surface, from $r=0$ mm to $r=10$ mm, using a refractive index matched analog fluid with a kinematic viscosity of 1.51 cSt. Details of the LDV system and acquisition can be found in Navitsky et al. (2014). Velocity realizations ($n=20{,}000$) are collected, and the 700 ms period is divided into 20 ms bins for analysis. There are more than 500 realizations per bin, which is sufficient to accurately calculate mean near-disc velocity throughout the cardiac cycle but can result in large error bars due to time averaging.

3. Computational methods

3.1. Model governing equations

We adopt a continuum approach throughout so that the laminar flow of a Newtonian fluid governed by Eqs. (1) and (2) are used to calculate the velocity ($\boldsymbol{u}$) and pressure (p) fields, where ρ is the density and ν is the kinematic viscosity.

$$\nabla \bullet \boldsymbol{u} = 0 \tag{1}$$

$$\frac{\partial \boldsymbol{u}}{\partial t} + (\boldsymbol{u} \bullet \nabla)\boldsymbol{u} = -\frac{1}{\rho}\nabla p + \nu \nabla^2 \boldsymbol{u} \tag{2}$$

Bulk concentrations of four species are calculated in each computational cell: non-activated platelets, activated platelets, SAPs, and adenosine diphosphate, ADP (a chemical activator). Platelet agonists or high shear stress can activate platelets either chemically or mechanically, respectively, and include ADP, thromboxane A_2, and thrombin; participating in feedback loops that continue to activate platelets even if the initial activating stimulus is removed. The proposed model focuses on ADP, which has been shown to be the primary chemical activator of platelets (Fogelson, 2008).

The concentrations of non-activated, ϕ_n, and activated, ϕ_a, platelets are calculated using Eqs. (3) and (4), respectively, based on Fogelson (1992) though the cohesive stress tensor was removed. Terms that are equal in magnitude but opposite in sign, $[A_C(ADP)]\phi_n + \left[A_M\left(\phi_f, \tau\right)\right](\phi_a + \phi_n)$, quantify the total rate of platelet activation (a sink for non-activated platelets and a source for activated platelets), based on chemical (A_C) and mechanical (A_M) stimuli, where τ is the shear stress and ϕ_f is the fraction of activated platelets in the system. This ensures that mass is conserved in the platelet population. The transport equations for non-activated and activated platelets are modified to account for the loss of platelets from both sub-populations as they adhere to a surface ($k_{ns}\phi_n$ and $k_{as}\phi_a$, respectively, where k_{ns} represents the reaction rate for non-activated platelets and k_{as} represents the activated platelet adhesion to a surface). While both sub-populations are allowed to adhere to a surface, any platelets that embolize from a surface are assumed to be in the activated state. Therefore, any platelets that are removed from a surface ($k_{off}\phi_{sa}$, where k_{off} is the reaction rate for the removal of platelets from a surface) are added to the activated platelet population. Eqs. (3) and (4) also include D_n and D_a, the diffusivity for non-activated platelets and activated platelets.

$$\frac{\partial \phi_n}{\partial t} + (\boldsymbol{u} \bullet \nabla)\phi_n = D_n \nabla^2 \phi_n - \left\{[A_C(\mathrm{ADP})]\phi_n + \left[A_M\left(\phi_f, \tau\right)\right](\phi_a + \phi_n)\right\} - k_{ns}\phi_n \tag{3}$$

$$\frac{\partial \phi_a}{\partial t} + (\boldsymbol{u} \bullet \nabla)\phi_a = D_a \nabla^2 \phi_a + \left\{[A_C(\mathrm{ADP})]\phi_n + \left[A_M\left(\phi_f, \tau\right)\right](\phi_a + \phi_n)\right\} - k_{as}\phi_a + k_{off}\phi_{sa} \tag{4}$$

Chemical platelet activation uses a function of ADP concentration $[A_C(\mathrm{ADP})]$, Eq. (5). This term is a linear rate equation with an activation threshold (ADP_t) and is identical to one used by Sorensen et al. (1999a). The rate of chemical platelet activation

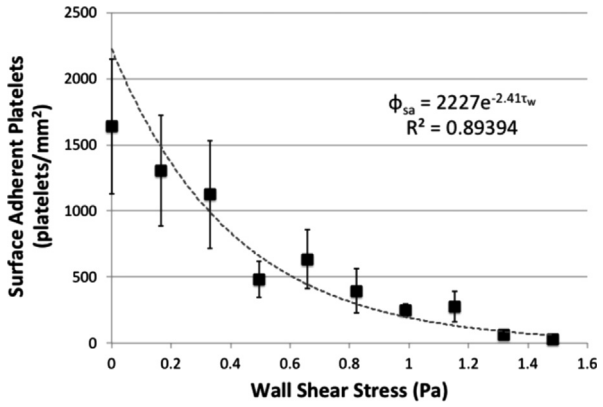

Fig. 2. Plot of asymptotic concentrations of SAPs versus WSS. Experimental data are from Navitsky et al. (2014) and are represented with black squares. The data were collected using a steady disc rotation of 283 RPM (29.63 rad/s). Error bars denote SEM. An exponential equation is fitted to the data and the equation and R^2 value are displayed.

also depends on a characteristic time, t_{ADP}.

$$A_C(\mathrm{ADP}) = \begin{cases} 0 & \text{for } \frac{\mathrm{ADP}}{ADP_t} < 1 \\ \frac{\mathrm{ADP}}{(ADP_t)(t_{ADP})} & \text{for } \frac{\mathrm{ADP}}{ADP_t} \geq 1 \end{cases} \tag{5}$$

Mechanical platelet activation, a function of both shear stress and exposure time, is not accounted for in Fogelson (1992). In the current model, mechanical activation $\left[A_M\left(\phi_f, \tau\right)\right]$ is quantified with a simplified form of a Lagrangian power law model proposed by Soares et al. (2013), given as Eq. (6), which requires empirically determined coefficients (C, α, and β) that can be estimated from in vitro or in vivo data. The scalar shear stress (τ), which gives a measure of the total shear stress based on the viscous stress tensor, is calculated following Bludszuweit (1994), and ϕ_f is the fraction of activated platelets in the system ($\phi_f = \phi_a/(\phi_a+\phi_n)$).

$$A_M\left(\phi_f, \tau\right) = \left(1-\phi_f\right) C^{\frac{1}{\beta}} \beta \phi_f^{\frac{\beta-1}{\beta}} \tau^{\frac{\alpha}{\beta}} \tag{6}$$

The concentration of ADP is tracked using Eq. (7), which modifies the chemical activator transport equation in Fogelson (1992) to include mechanical stimuli. Eq. (7) includes terms to account for temporal and spatial changes in ADP concentration. Production is solely due to the release of ADP by activated platelets $\left(R_{\mathrm{ADP}}\left\{[A_C(\mathrm{ADP})]\phi_n + \left[A_M\left(\phi_f, \tau\right)\right](\phi_a+\phi_n)\right\}\right)$, which preserves one of the primary feedback loops in the thrombotic process. Platelets store ADP in granules and release it upon activation, with the rate of ADP release calculated by multiplying the amount of ADP contained in a platelet (R_{ADP}) by the rate of platelet activation $\left\{[A_C(\mathrm{ADP})]\phi_n + \left[A_M\left(\phi_f, \tau\right)\right](\phi_a+\phi_n)\right\}$. D_{ADP} is the diffusivity for ADP.

$$\frac{\partial ADP}{\partial t} + (\boldsymbol{u}\bullet\nabla)\mathrm{ADP} = D_{ADP}\nabla^2 ADP + R_{ADP}\left\{[A_C(\mathrm{ADP})]\phi_n + \left[A_M\left(\phi_f, \tau\right)\right](\phi_a+\phi_n)\right\} \tag{7}$$

The transport equation for SAPs (ϕ_{sa}), Eq. (8), considers the adhesion of both non-activated (ϕ_n) and activated (ϕ_a) platelets to a material surface, and the embolization of adherent platelets. A weighting function (S_{sa}) limits the total number of activated platelets that can adhere to a surface, Eq. (10). The reaction rates and asymptotic number of SAPs ($\phi_{sa,max}$) are material dependent. Here, we use PUU. There is no diffusion or advection of SAPs.

$$\frac{\partial \phi_{sa}}{\partial t} = S_{sa}\left(k_{ns}\phi_n + k_{as}\phi_a\right) - k_{off}\phi_{sa} \tag{8}$$

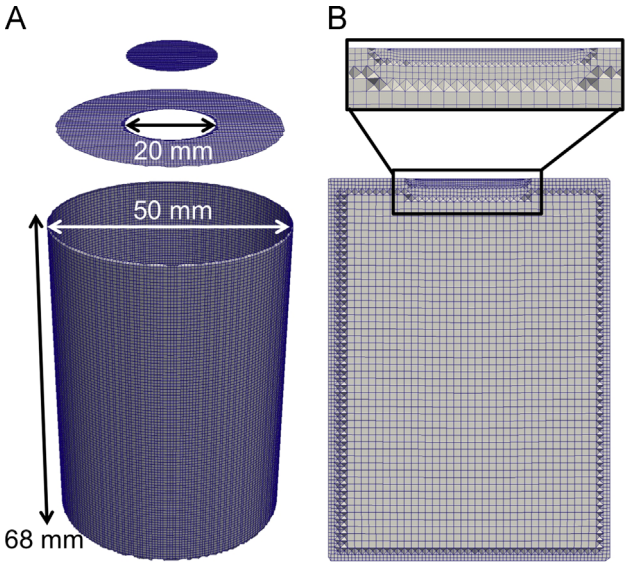

Fig. 3. The RDS mesh containing approximately 165,000 elements. (A) RDS mesh boundaries, from bottom to top: acrylic/fluid, air/fluid, and disc/fluid. (B) A centerline view of the internal (fluid) mesh in the RDS domain. A structured mesh is used away from boundaries, and an unstructured mesh is used at the boundaries. An expanded view of the mesh near the disc/fluid boundary shows the surface-normal mesh layers used to improve mesh resolution.

$$S_{sa} = 1 - \frac{\phi_{sa}}{\phi_{sa,max}} \tag{9}$$

The maximum number of SAPs is determined based on platelet adhesion to PUU using a rotating disc under steady conditions (Navitsky, 2014). In the in vitro study, adherent platelets were quantified after two hours of disc rotation, which ensured asymptotic surface platelet densities were reached (Neumann, 1980). Fig. 2 shows adherent platelets versus WSS. Using a best fit exponential equation from Fig. 1 to calculate $\phi_{sa,max}$ in Eq. (9), we obtain Eq. (10), where τ_w is the WSS.

$$S_{sa} = 1 - \frac{\phi_{sa}}{2227e^{-2.41\tau_w}} \tag{10}$$

3.2. RDS computational approach

The open-source CFD toolbox OpenFOAM, version 2.1.1, is used for the meshing and simulations. Three-dimensional hybrid meshes of hexahedral cells were created using the snappyHexMesh utility. The computational domain (Fig. 3A) is identical to the LDV acrylic model, that is, a 50 mm diameter cylinder with a height of 68 mm. The mesh has structured cells in the interior of the chamber, with unstructured cells near all boundaries (Fig. 3). Three surface-normal mesh layers are added at the disc/fluid boundary to improve the spatial resolution in the region of platelet adhesion. The near disc mesh layer has a thickness of 92.5 μm.

A no-slip velocity condition is imposed at the acrylic/fluid boundary, while a slip velocity condition is defined at the air/fluid boundary. A rotational velocity boundary condition is used at the disc/fluid boundary. Zero gradient boundary conditions are imposed at all boundaries for pressure. Initial concentrations of ADP and SAPs are defined as zero. The total platelet concentration is defined as 350×10^6 platelets/mL to match the bovine platelet rich plasma (PRP) platelet concentration used by Navitsky et al. (2014). The initial platelet concentration was set to 5%, which gives initial concentrations of 17.5×10^6 platelets/mL and 332.5×10^6 platelets/mL for activated and non-activated platelets, respectively. The diffusion coefficients for non-activated and

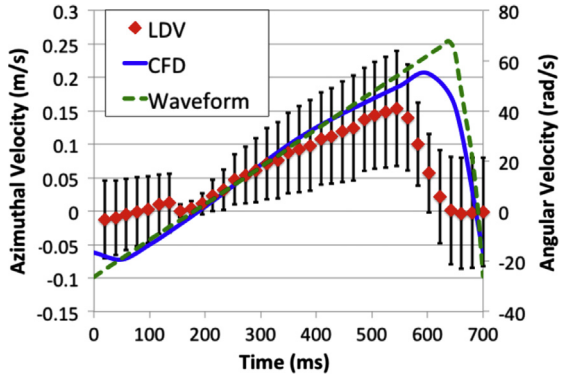

Fig. 4. Comparison of experimental (LDV) and computational azimuthal velocity (left vertical axis) for pulsatile disc rotation at a radial location of 5 mm and a depth of 100 μm beneath the disc. One waveform period is considered, and the LDV velocities are presented as bin mean ± bin S.D. Additionally, the pulsatile waveform is plotted on the right vertical axis. A small offset (approximately 50 ms) is observed between the LDV and CFD velocities due to difficulty triggering the LDV software precisely at the waveform minimum.

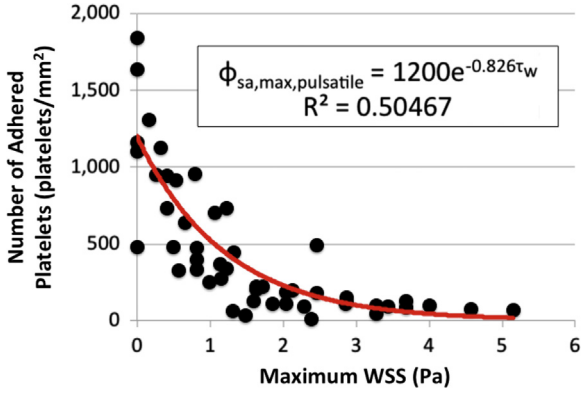

Fig. 5. Plot of asymptotic SAP concentrations versus maximum WSS under pulsatile conditions. The pulsatile in vitro results (Navitsky et al., 2014) are displayed as black circles and the exponential fit to the in vitro data is displayed as a solid red line. (For interpretation of the references to color in this figure legend, the reader is referred to the web version of this article.)

activated platelets are for normal Brownian motion: 1.58×10^{-9} cm^2/s (Goldsmith and Turitto, 1986).

A mesh independence study is conducted using Richardson extrapolation with the domain discretized using initial grids of four refinement levels: coarse, medium, fine, and finest (97,975, 163,183, 288,970, and 506,669, respectively). Simulations are performed at a steady rotation rate (29.63 rad/s) for 30 min of simulation, using time steps of 0.5 s. The integrated value of ϕ_{sa} on the disc surface is used as the parameter for Richardson extrapolation, as it gives a global measure of adherent platelets and prevents interpolation errors from influencing the results. Our medium mesh gave acceptable discretization error of less than 5%.

A time step independence study is conducted using the medium mesh with time steps of 6.25, 12.5, 25, and 50 ms (a constant refinement factor of 2). The integrated value of ϕ_{sa} on the disc surface after 5 min is used to quantify simulation results; however, in this case, the pulsatile waveform is used to control disc rotation. Time steps of 25 ms were found to be adequate for the pulsatile condition.

Fig. 4 shows the pulsatile flow comparison between the RDS waveform and LDV and CFD velocities.

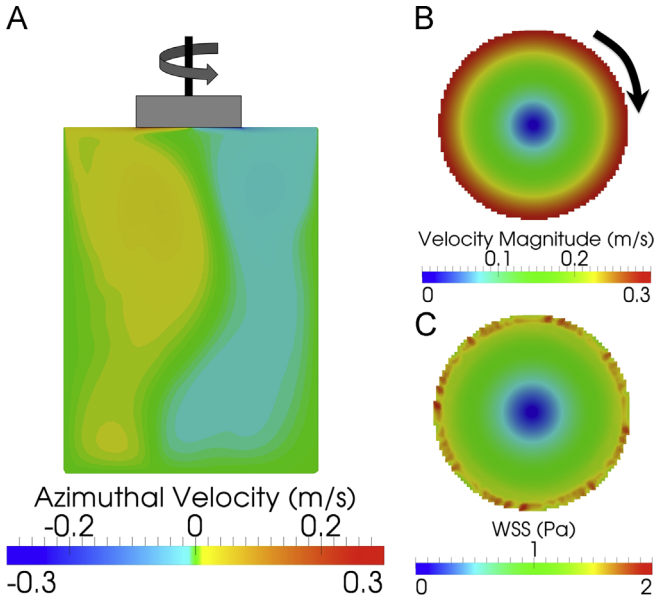

Fig. 6. Visualization of a steady RDS simulation (ω=29.63 rad/s). (A) Azimuthal velocity (positive is out of the page) plotted on a centerline cut through the domain. The color bar is compressed near zero to illustrate the large-scale velocity patterns present in the chamber, and a representation of the rotating disc is added to provide context (the physical disc is not modeled in the simulations, only the surface in contact with the fluid). (B) Velocity magnitude on the surface of the disk with an arrow showing the direction of disc rotation. (C) WSS distribution on the disc surface. Edge effects influence the WSS calculation near the disc edge and cause the "patchy" distribution near the edge.

3.3. Determination of model parameters

k_{ns}, k_{as}, and k_{off} must be determined in Eq. (8). First, a sensitivity analysis is conducted to determine values of k_{ns} and k_{as}, which allow the concentration of SAPs to approach asymptotic levels at a reasonable rate. Navitsky et al. (2014) only investigated asymptotic densities of adherent platelets, thus the work of Neumann et al. (1980) is used. As Neumann et al. (1980) used static conditions (zero shear), we require SAPs concentrations at the disc center to be within 5–10% of their asymptotic values after one hour of steady disc rotation. Sorensen et al. (1999b) determined that the adhesion rate of activated platelets to collagen was 25% greater than the adhesion rate of non-activated platelets to collagen, and their result is used to reduce the two-variable sensitivity study to a one-variable sensitivity study ($1.25k_{ns} = k_{as}$).

When Navitsky et al. (2014) investigated platelet adhesion under pulsatile conditions, they found the asymptotic concentrations were dependent on the maximum WSS at a given location. Asymptotic adherent platelet concentrations are plotted versus maximum WSS in Fig. 5. The exponential fit gives the expected asymptotic concentration of SAPs ($\phi_{sa,max,pulsatile}$) based on the maximum WSS over a pulsatile cycle, and is used in an algorithm to determine whether there is a local increase or a decrease in SAPs at a boundary based on the local WSS and the current SAP concentration. The algorithm includes the WSS field, the local WSS to determine the asymptotic adherent platelet concentration, and the local adherent platelet concentration.

4. Results

4.1. Determination of model parameters and steady RDS simulation

Simulations are performed for adhesion rates (k_{as}) from 5×10^{-12} to 5×10^{-8} m/s, with k_{off} zero. The simulation with $k_{as} = 5 \times 10^{-9}$ m/s

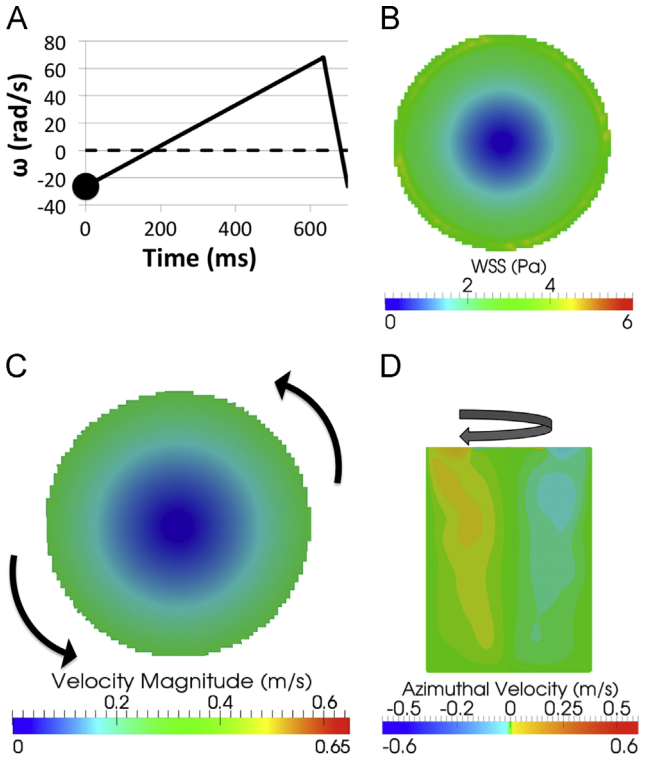

Fig. 7. Simulation results 0 ms into the waveform period, as indicated in (A). A dotted black line marks zero rotation. (B) WSS distribution on the disc surface. (C) Velocity magnitude on the disc surface, and the direction of rotation indicated with black arrows. (D) Azimuthal velocity across a centerline cut of the RDS domain. The color scale is compressed near zero to better illustrate low velocity circulation and positive velocity is out of the screen. Disc rotation is indicated with an arrow above the color plot.

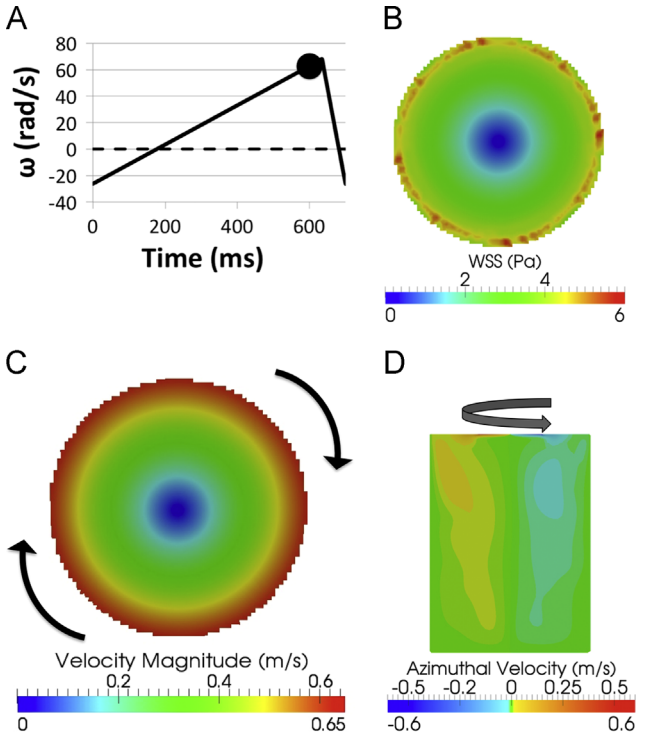

Fig. 8. Simulation results 600 ms into the waveform period, as indicated in (A). A dotted black line marks zero rotation. (B) WSS distribution on the disc surface. (C) Velocity magnitude on the disc surface, and the direction of rotation indicated with black arrows. (D) Azimuthal velocity across a centerline cut of the RDS domain. The color scale is compressed near zero to better illustrate low velocity circulation and positive velocity is out of the screen. Disc rotation is indicated with an arrow above the color plot.

produces a SAP concentration in line with the results of Neumann et al. (1980). Accordingly, k_{as} is 5×10^{-9} m/s.

The steady flow field in the chamber, disc velocity distribution, and disc WSS distribution are illustrated in Fig. 6, where the maximum velocities and WSS are found near the disc edge. Much of the velocity is near zero away from the disc, but there is a low velocity circulation (< 0.05 m/s) in the chamber.

4.2. Pulsatile RDS simulations

The initial value for k_{off} is defined as 5×10^{-2}, seven orders of magnitude greater than k_{as}. The azimuthal velocity in the reservoir, disc velocity, and disc WSS are displayed for peak counterclockwise (Fig. 7) and clockwise (Fig. 8) rotation. The disc rotation changes direction between 100 and 200 ms and between 600 and 700 ms during the cycle. The maximum disc WSS corresponds to the maximum disc rotation rate, which produces disc velocities exceeding 0.6 m/s.

Predicted SAP concentration profiles reach their asymptotic values faster near the edge of the disc. However, radial locations near the center reach asymptotic concentrations faster. The platelet concentration at the disc center reaches its asymptotic value ($\sim$1000 platelets/mm^2) after 20 min, while the same location needed over one hour to reach the asymptotic concentration ($\sim$2000 platelets/mm^2) under steady conditions. The time required for the a SAP concentration (0 to 1000 platelets/mm^2) is much less than the time required from 1000 to 2000 platelets/mm^2 because of the limiting function given as Eqs. (9) and (10). Consequently, as the Fig. 5 trendline predicts a lower asymptotic SAP concentration at the center than the Fig. 1 trendline, platelet adhesion is arrested near the disc center. This phenomenon does not occur at greater radial locations, where the trendline in Fig. 5 predicts greater platelet concentrations.

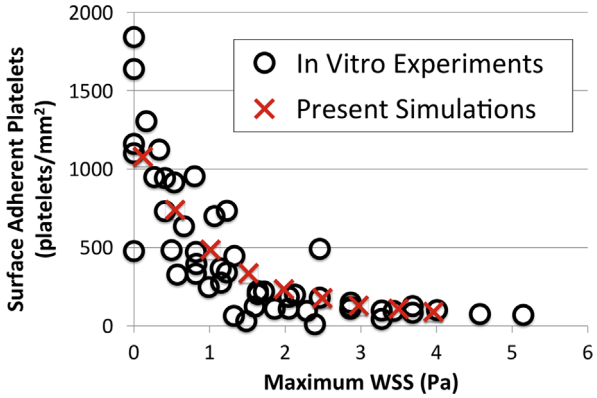

Fig. 9. Present pulsatile simulation results after one hour compared to the pulsatile in vitro results of Navitsky et al. (2014), with adherent platelet concentrations plotted as a function of maximum WSS over the waveform period.

The predicted asymptotic concentrations are also plotted along with the pulsatile in vitro data of Navitsky et al. (2014) in Fig. 9. Nice agreement is observed between the computations and the aggregation of the pulsatile in vitro data, but this is expected, as the trendline in Fig. 5 is determined from the same data presented in Fig. 9.

5. Discussion

The SAP equation is developed and used in CFD simulations. The equation considers WSS-dependent adhesion of non-activated

and activated platelets, along with the WSS-dependent embolization of activated platelets, and it is incorporated into a continuum platelet aggregation model (Fogelson, 1992). Based on the in vitro study, the pulsatile waveform produced the highest peak disc angular velocity, and the highest disc WSS. This allows the developed adherent platelet equation to be tested under the most extreme shearing conditions from the in vitro study (Navitsky, 2014).

Device developers may need to consider a range of blood hematocrits, and thus blood viscosities, when evaluating device performance, as hematocrit varies amongst animal species (Windberger et al., 2003) and patient ages (Linderkamp et al., 1984). Additionally, whole blood is often modeled as a Newtonian fluid, though it is a shear-thinning non-Newtonian fluid. Any simulation using a non-Newtonian model for blood viscosity will likely produce a range of fluid viscosities, and large differences in peak WSS have been calculated when Newtonian and non-Newtonian blood simulations are compared (Good et al., 2015). If the present results are extrapolated to whole blood, it is reasonable to conclude there would be fewer platelets adhered to the disc surface (when compared to PRP with an identical platelet concentration) based solely on the increase in WSS due to an increased viscosity. However, this is contrary to Grunenwald (2013), who found adhered platelet densities an order of magnitude greater when whole blood was used in place of PRP. These results indicate that the enhanced diffusivity of platelets due to red blood cells increases platelet adhesion by a greater amount than the heightened WSS decreases platelet adhesion. This behavior was also found by Zydney and Colton (1988).

There is no appreciable platelet activation or ADP accumulation predicted in the present simulations. Fluid stresses remain low throughout the entire computational domain, resulting in little mechanical platelet activation and little ADP production. This leaves the initial background level of platelet activation as the primary determinant of activated platelet concentration. Even though no analyses are conducted to test the model sensitivity to background platelet activation, it is unlikely that adherent platelet predictions will be significantly affected. The term for platelet adhesion per unit time, $S_{sa}(k_{ns}\phi_n + k_{as}\phi_a)$ in Eq. (8), can be rewritten as Eq. (11), where ϕ_p is the total free platelet concentration (i.e. $\phi_p = \phi_n + \phi_a$) and BA is the background level of platelet activation (0.05 in the present study).

$$S_{sa}(k_{ns}\phi_n + 1.25k_{ns}\phi_a) = S_{sa}k_{ns}\left[(1-\mathrm{BA})\phi_p + 1.25(\mathrm{BA})\phi_p\right] \tag{11}$$

Background levels of platelet activation have been reported from 0.01 (Goodman et al., 2005) to nearly 0.2 (Kennedy et al., 1997), and these extremes can be used to estimate the maximum sensitivity of the model to BA. If BA=0.01, the platelet adhesion rate is calculated as $S_{sa}k_{ns}\left[(.99)\phi_p + 1.25(0.01)\phi_p\right] = S_{sa}k_{ns}(1.0025)\phi_p$; conversely, if BA=0.2, the platelet adhesion rate is calculated as $S_{sa}k_{ns}\left[(0.8)\phi_p + 1.25(0.2)\phi_p\right] = S_{sa}k_{ns}(1.05)\phi_p$. These two adhesion rates differ by less than 5%, and the difference will decrease as the SAP concentration increases and S_{sa} approaches zero. Additionally, changes in BA do not affect asymptotic platelet levels, only the predicted rate at which platelets adhere to a surface. Finally, the values for k_{as} and k_{ns}, from Sorensen et al. (1999b), are approximately four orders of magnitude greater than the rates determined. However, they studied platelet adhesion to a highly reactive surface, collagen, while the present study uses a biomaterial known for only eliciting a small platelet response.

There are noteworthy differences in the trendlines fit to the steady and pulsatile in vitro data. Fig. 10 highlights the differences in their predicted asymptotic adherent platelet concentrations over a range of WSS. The steady trendline predicts higher asymptotic concentrations at low WSS, while the pulsatile predicts higher asymptotic concentrations at high WSS. The differences result in a region where the WSS is simultaneously too high for new platelets to adhere to a surface and too low for platelets to be removed from the surface (blue horizontal lines in Fig. 10). This region causes the asymptotic behavior radially over specific temporal periods of the cardiac cycle. Conversely, there is a low shear region (<0.4 Pa) where both platelet adhesion and platelet embolization are predicted (red vertical lines in Fig. 10). The former region is reasonable, as platelets form strong bonds to a surface after initial adhesion; however, the latter region does not and a larger experimental sample size may be required to calculate more accurate trendlines. Better agreement in the low shear region will also result in more realistic platelet adhesion curves with increasing time. Currently, radial locations near the disc center, such as $r=2$ mm, experience an abrupt arrest of platelet adhesion once the pulsatile asymptotic value is reached due to the disagreement between the two trendlines. Moreover, the trendline in Fig. 5 has an R^2 value of only 50%. There are likely additional predictive factors besides maximum WSS throughout the cycle, such as surface exposure time to a given WSS, that are important for platelet adhesion in pulsatile flow, and future work will help elucidate these relationships to improve the model.

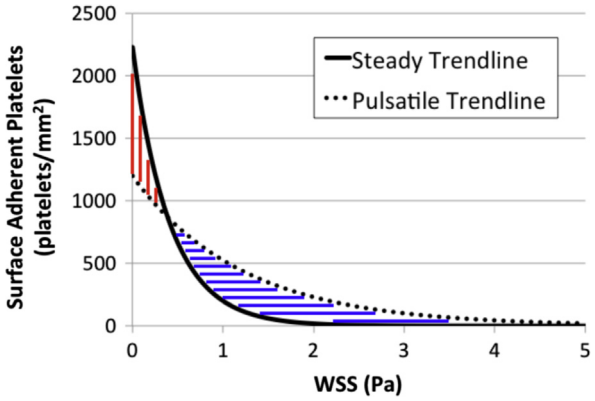

Fig. 10. Differences in predicted asymptotic adherent platelet densities between the trendlines for steady and pulsatile platelet adhesion data (Navitsky et al., 2014). Regions where the steady trendline predicts higher asymptotic adherent platelet concentrations are highlighted with vertical red lines, while regions where the pulsatile trendline predicts higher asymptotic adherent platelet concentrations are highlighted with horizontal blue lines. The trendlines are equal at approximately 0.4 Pa. (For interpretation of the references to color in this figure legend, the reader is referred to the web version of this article.)

Our present work focuses on laminar flow conditions, even though a wide range of medical devices are designed for implantation into the high Re flow of the arterial circulation (e.g., stents, prosthetic heart valves, and ventricular assist devices). Heightened platelet adhesion and accumulation has been found under pathological shear conditions (Jurk et al., 2003; Ruggeri et al., 2006; Bark et al., 2012), but our governing equations are currently not formulated to make predictions in turbulent flow. Yet, our model framework allows for the addition of future terms, particularly for platelet activation in response to turbulent stresses, which are necessary for simulation of device-induced thrombosis in high Re flow. Nevertheless, we feel it is imperative to demonstrate model success under laminar conditions before advancing to the more complex fluid mechanics associated with turbulence.

Lastly, the extension of the platelet adhesion aspect of the model to a wider range of materials needs to be considered. The methodology we have presented, along with published work for existing biomaterials or preliminary blood-contacting data for novel biomaterials, provides a way to estimate SAP trendlines and, subsequently, calibrate a SAP transport equation for computational simulations.

6. Conclusions

An RDS is simulated to develop and calibrate a transport equation for SAPs to PUU. The equation is developed with the help of platelet adhesion data from (Navitsky, 2014), and the equation is added to an Eulerian platelet activation and adhesion model. The simulated velocities and WSSs show excellent agreement with LDV results under steady and pulsatile conditions. After determining model coefficients through a sensitivity analysis, the platelet adhesion model is tested under the most extreme shearing conditions from the in vitro study. When presented alongside an aggregate of all in vitro pulsatile platelet adhesion results, the computational predictions show nice agreement. As platelet adhesion can be a precursor to macroscopic thrombus development, platelet adhesion has been used as a metric to assess the efficacy of blood-contacting devices (Topper et al., 2014). The presented equation for SAPs, incorporated into a larger model of device-induced thrombosis, provides device developers with an improved tool to cheaply and quickly evaluate blood-contacting device performance.

Conflict of interest statement

The authors have no conflicts of interest to disclose.

Acknowledgments

A Walker Graduate Assistantship from the Applied Research Laboratory at the Pennsylvania State University and a Penn State Grace Woodward Foundation grant supported this work.

References

Bark, D.L., Para, A.N., Ku, D.N., 2012. Correlation of thrombosis growth rate to pathological wall shear rate during platelet accumulation. Biotechnol. Bioeng. 109 (10), 2642–2650.
Bludszuweit, C., 1994. A Theoretical Approach To The Prediction of Haemolysis In Centrifugal Blood Pumps (PhD. Thesis). University of Strathclyde, Strathclyde.
Cito, S., 2013. Review of macroscopic thrombus modeling methods. Thromb. Res. 131, 116–124.
Daemen, J., Wenaweser, P., Tsuchida, K., Abrecht, L., Vaina, S., Morger, C., Kukreja, N., Jüni, P., Sianos, G., Hellige, G., van Domburg, R.T., Hess, O.M., Boersma, E., Meier, B., Windecker, S., Serruys, P.W., 2007. Early and late coronary stent thrombosis of sirolimus-eluting and paclitaxel-eluting stents in routine clinical practice: data from a large two-institutional cohort study. Lancet 369, 667–678.
deBiasi, A.R., Manning, K.B., Salemi, A., 2015. Science for surgeons: understanding pump thrombogenesis in continuous-flow left ventricular assist devices. J. Thor. Cardiol. Surg. 149, 667–673.
Fogelson, A.L., 1992. Continuum models of platelet aggregation: formulation and mechanical properties. SIAM J. Appl. Math. 52, 1089–1110.
Fogelson, A.L., Guy, R.D., 2008. Immersed-boundary-type models of intravascular platelet aggregation. Comput. Methods Appl. Mech. Eng. 197, 2087–2104.
Goldsmith, H.L., Turitto, V.T., 1986. Rheological aspects of thrombosis and haemostasis: basic principles and applications. Thromb. Haemost. 55, 415–435.
Good, B.C., Deutsch, S., Manning, K.B., 2015. Hemodynamics in a pediatric ascending aorta using a viscoelastic pediatric blood model. Ann. Biomed. Eng. 44, 1019–1035.
Goodman, P.D., Barlow, E.T., Crapo, P.M., Mohammad, S.F., Solen, K.A., 2005. Computational model of device-induced thrombosis and thromboembolism. Ann. Biomed. Eng. 33, 780–797.
Grunenwald, L.E., 2013. The Effects of Hematocrit and Rotation Time on Platelet Adhesion to a Polyurethane Urea Surface (Masters thesis). The Pennsylvania State University, University Park.
Jurk, J., Clemetson, K.J., de Groot, P.G., Brodde, M.F., Steiner, M., Savion, N., Varon, D., Sixma, J.J., Van Aken, H., Kehrel, B.E., 2003. Thrombospondin-1 mediates platelet adhesion at high shear via glycoprotein Ib (GPIb): an alternative/backup mechanism to von Willebrand factor. FASEB J. 17 (11), 1490–1492.
Kennedy, S.D., Igarashi, Y., Kickler, T.S., 1997. Measurement of in vitro P-selectin expression by flow cytometry. Am. J. Clin. Pathol. 107, 99–104.
Leiderman, K., Fogelson, A.L., 2014. An overview of mathematical modeling of thrombus formation under flow. Thromb. Res. 133, S12–S14.
Linderkamp, O., Versmold, H.T., Riegel, K.P., Betke, K., 1984. Contributions of red cells and plasma to blood viscosity in preterm and full-term infants and adults. Pediatrics 74, 45–51.
Marchena, E.D., Mesa, J., Pomenti, S., Marin Y Kall, C., Marincic, X., Yahagi, K., Ladich, E., Kutys, R., Aga, Y., Ragosta, M., Chawla, A., Ring, M.E., Virmani, R., 2015. Thrombus formation following transcatheter aortic valve replacement. J. Am. Coll. Cardiol. Int. 8, 728–739.
Mehra, M.R., Stewart, G.C., Uber, P.A., 2014. The vexing problem of thrombosis in long-term mechanical circulatory support. J .Heart Lung Transplant. 33, 1–11.
Milner, K.R., Snyder, A.J., Siedlecki, C.A., 2006. Sub-micron texturing for reducing platelet adhesion to polyurethane biomaterials. J. Biomed. Mater. Res. 76A, 561–570.
Mori, D., Yano, K., Tsubota, K.I., Ishikawa, T., Wada, S., Yamaguchi, T., 2008. Simulation of platelet adhesion and aggregation regulated by fibrinogen and von Willebrand factor. Thromb. Haemost. 99 (1), 108–115.
Navitsky, M.A., Taylor, J.O., Smith, A.B., Slattery, M.J., Deutsch, S., Siedlecki, C.A., Manning, K.B., 2014. Platelet adhesion to polyurethane urea under pulsatile flow conditions. Artif. Organs 38, 1047–1053.
Neumann, A.W., Hum, O.S., Francis, D.W., 1980. Kinetic and thermodynamic aspects of platelet adhesion from uspension to various substrates. J. Biomed. Mater. Res. 14, 499–509.
Ruggeri, Z.M., Orje, J.N., Habermann, R., Federici, A.B., Reininger, A.J., 2006. Activation-independent platelet adhesion and aggregation under elevated shear stress. Blood 106 (6), 1903–1910.
Soares, J.S., Sheriff, J., Bluestein, D., 2013. A novel mathematical model of activation and sensitization of platelets subjected to dynamic stress histories. Biomech. Model Mechanobiol. 12, 1127–1141.
Sorensen, E.N., Burgreen, G.W., Wagner, W.R., Antaki, J.F., 1999a. Computational simulation of platelet deposition and activation: i. Model. Dev. Prop. Ann. Biomed. Eng. 27, 436–448.
Sorensen, E.N., Burgreen, G.W., Wagner, W.R., Antaki, J.F., 1999b. Computational simulation of platelet deposition and activation: ii. results for Poiseuille flow over collagen. Ann. Biomed. Eng. 27, 449–458.
Stewart, S.F.C., Hariharan, P., Paterson, E.G., Burgreen, G.W., Reddy, V., Day, S.W., Giarra, M., Manning, K.B., Deutsch, S., Berman, M.R., Myers, M.R., Malinauskas, R.A., 2013. Results of FDA's first interlaboratory computational study of a nozzle with a sudden contraction and conical diffuser. Cardiol. Eng. Technol. 4, 374–391.
Strong, A.B., Stubley, G.D., Chang, G., Absolom, D.R., 1987. Theoretical and experimental analysis of cellular adhesion to polymer surfaces. J. Biomed. Mater. Res. 21, 1039–1055.
Taylor, J.O., Meyer, R.S., Deutsch, S., Manning, K.B., 2016. Development of a computational model for macroscopic predictions of device-induced thrombosis. Biomech. Model Mech. Biol. (Online)
Taylor, J.O., Witmer, K.P., Neuberger, T., Craven, B.A., Meyer, R.S., Deutsch, S., Manning, K.B., 2014. In vitro quantification of time dependent thrombus size using magnetic resonance imaging and computational simulations of thrombus surface shear stresses. J. Biomech. Eng. 136 (071012-1-11).
Tokarev, A.A., Butylin, A.A., Ataullakhanov, F.I., 2011. Platelet adhesion from shear blood flow is controlled by near-wall rebounding collisions with erythrocytes. Biophys. J. 100 (4), 799–808.
Topper, S.R., Navitsky, M.A., Medvitz, R.B., Paterson, E.G., Siedlecki, C.A., Slattery, M. J., Deutsch, S., Rosenberg, G., Manning, K.B., 2014. The use of fluid mechanics to predict regions of microscopic thrombus formation in pulsatile VADs. Cardiol. Eng. Tech. 5, 54–69.
Wang, W., King, M.R., 2012. Multiscale modeling of platelet adhesion and thrombus growth. Ann. Biomed. Eng. 40, 2345–2354.
Windberger, U., Bartholovitsch, A., Plasenzotti, R., Korak, K.J., Heinze, G., 2003. Whole blood viscosity, plasma viscosity and erythrocye aggregation in nine mammalian species: reference values and comparison of data. Exp. Physiol. 88, 431–440.
Xu, Z., Kamocka, M., Alber, M., Rosen, E.D., 2011. Computational approaches to studying thrombus development. Arterioscler. Thromb. Vasc. Biol. 31, 500–505.
Yamanaka, H., Rosenberg, G., Weiss, W.J., Snyder, A.J., Zapanta, C.M., Siedlecki, C.A., 2005. Multiscale analysis of thrombosis in left ventricular assist systems. ASAIO J. 51, 567–577.
Zydney, A.L., Colton, C.K., 1988. Augmented solute transport in the shear flow of a concentrated suspension. Physicochem. Hydrodyn. 10, 77–96.